Brief Review

Modern Physics Letters A
Vol. 22, No. 33 (2007) 2479–2492

World Scientific
www.worldscientific.com

PROGRESS IN THE STUDY OF THE γ-DECAY OF THE GIANT DIPOLE RESONANCE IN HOT NUCLEI

A. BRACCO, F. CAMERA and O. WIELAND*

University of Milano and INFN sez. of Milano, Via Celoria 16, 20133 Milano, Italia
**oliver.wieland@mi.infn.it*

W. E. ORMAND

Lawrence Livermore National Laboratory, Livermore, USA
nuclear.structure@mi.infn.it

Received 10 August 2007

The problem of the damping of the Giant Dipole Resonance (GDR) at finite temperature at $T > 2$ MeV is discussed here. The experimental results are based on fusion evaporation reactions. The most recent results on the mass region $A = 132$ (Ce isotopes) obtained in exclusive measurements are compared with the existing results on the $A = 110$–120 region (Sn isotopes). The comparison with the theoretical predictions based on thermal shape fluctuations is also discussed. The GDR width is found to increase also in the region $T > 2$ MeV and this is accounted by the combined effect of the increase of the compound nucleus width (smaller lifetime) and to the increase of the average deformation of the nucleus.

Keywords: GDR; hot nuclei; statistical model.

PACS Nos.: 21.10.Pc, 21.10.Re, 21.60.Ev, 21.60.Ka, 23.20.Lv, 27.20.+q

1. Introduction

The investigation of the properties of the Giant Dipole Resonance (GDR) at high temperature and angular momentum provides an insight into the behavior of nuclei under extreme conditions. The wealth of experimental data on this subject covers in most cases the interval of temperatures up to ≈ 2.5 MeV. These data are based on the study of the γ-decay of hot rotating Compound Nuclei formed mainly using fusion-evaporation reactions. The measured systematics on the GDR width shows consistently a rapid increase of the GDR width and have been shown to provide an important testing ground for the theoretical models for damping of collective modes at finite temperature. In general[1–7] the change of the GDR width with angular momentum and temperature is found to be induced mainly by the large amplitude thermal fluctuations of the nuclear shape while quanta fluctuations do not seem to play a relevant role. In particular the small amplitude quanta fluctuations, induced

by nucleon–nucleon collisions could start affecting the GDR width at the highest temperature (3–4 MeV). It is clear that while at $T < 2$ MeV we have a rather good picture on the problem of the damping of the GDR, at higher temperatures the situation is more complex. In fact, the experimental study at $T > 2$ MeV could suffer from the problem of the incomplete thermalization of the nucleus, basic property that the nucleus must have when the dipole oscillation is built on it. This important problem has been raised in the works[8,9] on Sn isotopes. In particular that works have shown that in the case of Sn at excitation energies $E^* > 150$ MeV the temperature of the γ-ray emitting systems had to be corrected with respect to that given by the kinematics of the complete fusion reaction to take into account the pre-equilibrium emission. The case of Sn isotopes at temperature up to ≈ 2.5 MeV using the reaction $^{18}\mathrm{O} + {}^{100}\mathrm{Mo}$ with $E_{\mathrm{beam}} = 122$–217 MeV was particularly instructive. In fact the analysis of the light charged particle (LCP) spectra has shown that the pre-equilibrium contribution is sizable, corresponding, in the case of the highest bombarding energies, to a loss of excitation energy of approximately 20%. Based on that result corrections for the determination of the temperature of the emitting nucleus were applied also for data leading to the same compound but using different projectile target combinations. Only in a few cases the applied correction was verified by the interpretation of the α (and/or other) particle spectra emitted in the same reaction, in other cases it was extrapolated by systematics. One point that should be mentioned that most of the work was based on data points corresponding to rather inclusive measurements without the detection of the recoiling residual nuclei.[8–14] This reinterpretation of the existing data reported from Kelly *et al.*,[8,9] motivated by the effort of defining well the excitation energy of the compound affecting the GDR analysis, provided a picture of the temperature dependence of the GDR width no longer consistent with the previous one indicating saturation effects in the damping mechanisms. In fact, the obtained picture before the analysis of Kelly evidenced that beyond the bombarding energy at which the angular momentum saturates, the GDR width increases slowly reflecting the fact that the nuclear deformation increase induced by temperature is milder than that induced by angular momentum. In contrast the results of Kelly *et al.*[8,9] showed a continuous increase of the GDR width when the values of the excitation energies were corrected for the pre-equilibrium emission. However, one weak point of the work on Sn is that only few data points were obtained in exclusive measurements and that the correction of the temperature of the data point was measured only in the case of the reactions induced by oxygen beams. Consequently, the behavior of the GDR at the highest temperatures ($T > 2.0$ MeV) could be considered as an interesting problem more complex than expected. To obtain a better insight of the problem, further measurements were made in another nucleus in the nearby mass region $A = 132$. As the chosen Ce isotopes are in the same mass region as the Sn isotopes, a similar behavior for the width increase induced by temperature is expected. The important feature of the measurements for Ce is that both the γ-decay, and also α and proton decay spectra, all in coincidence with the recoiling

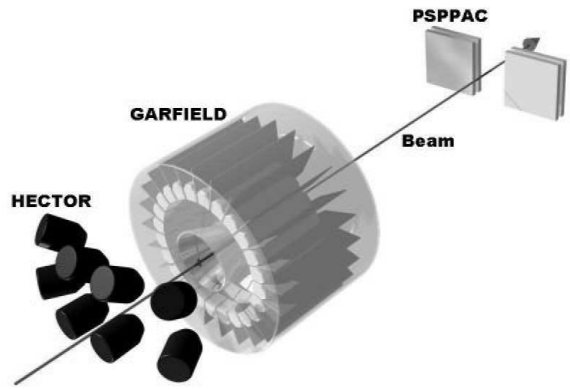

Fig. 1. A schematic drawing of the experimental setup. The arrow gives the direction of the pulsed beam from the accelerator. The target is placed at the entrance of the cylinder representing the GARFIELD array. The BaF_2 scintillators (HECTOR array) are placed at backward angles. The GARFIELD array covers the forward angle part of the setup. In the figure the 24 sectors, each consisting of ΔE gas microstrip detectors followed by to CsI(Tl) crystals are shown. The PSPPAC system (shown as double plates) covers the forward angles between 4° and 12°.

evaporation nuclei were obtained in the same experimental setup.[15–17] In addition, in order to find the most favorable experimental conditions leading to negligible pre-equilibrium contribution in the compound system formation, two different reactions were investigated. This is an important point since the evaluation of the pre-equilibrium contribution is model-dependent.

This paper discusses the results of the GDR width in Ce nuclei at $T > 2$ MeV and their comparison with the data on Sn isotopes. While a partial account of the data can be found in Refs. 15–17, here we discuss in more detail the experiment and the results on the GDR width.

2. Experiment

The experiments concerning the GDR study in the hot Ce nuclei were performed at the INFN National Laboratory of Legnaro. Two reactions were used, $^{64}Ni + {}^{68}Zn$ at beam energy of 300, 400 and 500 MeV and $^{16}O + {}^{116}Sn$ at beam energy of 130 and 250 MeV. The beams were accelerated with the TANDEM-ALPI complex. The kinematics for these reactions under the assumption of full linear momentum transfer give in the case of the ^{64}Ni beam an excitation energy of 100, 150 and 200 MeV, while for the ^{16}O beams an excitation energy of 100 and 150 MeV. The experimental setup used in these experiments consists of the combination of three detector systems. The first is the GARFIELD array[18] for the measurement of charged particles, the second is the HECTOR setup made of large volume BaF_2 detectors[19] and the third is a set of two Position Sensitive Parallel Plate Avalanche Counter telescopes (PSPPAC). A schematic drawing of the experimental setup is shown in Fig. 1.

The GARFIELD apparatus is a large acceptance system made by two drift chambers and it was specially designed to study nuclear processes in the low and intermediate energy range (5–20 MeV/u) heavy-ion induced reactions. In the experiments described in this work, only the forward chamber was mounted, covering an angular range from $\theta = 29^\circ$ to $\theta = 82^\circ$ and 2π in ϕ. The GARFIELD drift chamber, filled with CF4 gas at low pressure (50–70 mbar), is azimuthally divided into 24 sectors, and each sector consists of 8 $E - \Delta E$ telescopes, for a total of 192 telescopes. More specifically the ΔE signal is given by the drift chamber, where gaseous micro-strip detectors collect and amplify the primary electrons produced along the ionization track of the detected particle. The advantages of using micro-strip gas chambers are in the large dynamical range and in the high signal-to-noise ratio (Z identification from low energy protons up to highly ionizing heavy ions). The CsI(Tl) scintillation detectors, lodged in the same gas volume, are used to measure the residual energy E of the detected light ions. The calibration of the GARFIELD detectors was performed using elastically scattered ^{12}C and ^{16}O ions from a ^{181}Ta target at a number of bombarding energies in the interval from 6 to 20 MeV/u.

The recoiling heavy nuclei produced in the reactions were selected using two pairs of Position Sensitive Parallel Plate Avalanche Counters (PSPPACs). Each pair consists of two PSPPACs positioned the one behind the other and with a degrader (25 μm of Upilex) in between to stop the slow products. In this way the fusion-evaporation events were identify through the anti-coincidences between the two pairs of PSPPACs and through the Time Of Flight (TOF) measurement relative to the pulsed beam signal. The time resolution of the pulsed beam was better than 1 ns. The TOF measurement provided a precise discrimination between the fusion events and other reaction channels corresponding to reaction products with higher velocities. The core of the PSPPAC consists of a central cathode made of a 1.5 μm double-aluminized Mylar foil and of two anode plains, one perpendicular to the other, made of 200 parallel golden tungsten wires. The wires of the anode plane have a 20 μm diameter and are positioned at a distance of 1 mm from each other. The PSPPACs used in our experiment were assembled in a square shape with an active area of 400 cm^2. They were positioned at the distance of 150 cm from the target in order to cover the angular range from $\theta = 4^\circ$ to $\theta = 12^\circ$. The PSPPACs were operated with heptane vapor at 350 Pa and were kept in continuous flow to prevent ageing effects. The position resolution of the PSPPAC is less than 0.1°, and the time resolution is around 1 ns.

In Fig. 2(b) the measured TOF spectrum corresponding to the reaction ^{16}O + ^{116}Sn at $E_{\rm lab} = 250$ MeV is shown. One can note clearly that the narrow peak associated to the beam like particles is well separated from the heavy residues characterized by a much broader velocity distribution.

HECTOR consists of 8 large (14.5 × 17 cm) BaF_2 scintillators for the measurement of high energy γ-rays. In this experiment the detectors were placed inside the large GARFIELD scattering chamber at backward angles between 125° and 160°

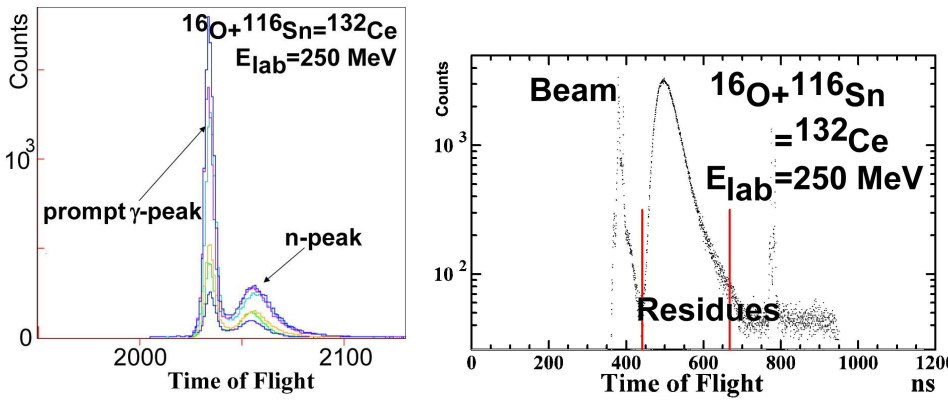

Fig. 2. (a) TOF spectra measured with the BaF_2 detectors positioned at 30 cm distance from the target (with 0.1 ns per channel). (b) The TOF spectrum measured with the PSPPAC detectors for the reaction $^{16}O + ^{116}Sn$ at $E_{lab} = 250$ MeV. The narrow peak is due to beamlike events while the broad peak (selected with two vertical lines) is due to the fusion-like residues events.

at $\approx$ 30 cm from the target. For these measurements, all the voltage dividers of the scintillators have been placed externally from the scattering chamber to avoid overheating of the electronics. At that distance from target it was possible to reject neutrons detected in BaF_2 by TOF measurements. In fact, the measured BaF_2 time resolution with respect to the pulse beam signal was $\simeq$ 1 ns, sufficient to identify γ-rays from neutrons. The neutrons arrive a few ns after the prompt γ-rays. This is shown in Fig. 2(a) displaying the measured TOF spectra measured for the reactions $^{16}O + ^{116}Sn$ at $E_{lab} = 250$ MeV. An electronic threshold of $\approx$ 4 MeV was set for γ-rays in order to reduce the acquisition dead-time due to the very high count rates of low energy γ-rays. The BaF_2 detectors were calibrated using standard γ-ray sources and the 15.1 MeV γ-rays from the reaction $d(^{11}B, n\gamma)^{12}C$ at beam energy of 19.1 MeV.

For all the measured reactions, the trigger condition required a coincidence of signals from PSPPACs and an OR between charged particle in the GARFIELD array and a signal in the BaF_2 detectors. In addition, we have also registered scaled down counts from the PSPPACs, GARFIELD and BaF_2 detectors in single mode. In order to monitor the beam intensity, we have used a Faraday cup, located downstream approximately 2 meter from the target center.

3. Experimental Results

The γ-ray spectra measured in coincidence with the heavy recoiling residual nuclei formed in the fusion reaction, are shown in Fig. 3 with the filled square points. A condition on the TOF spectrum, rejecting neutrons, was also applied to obtain

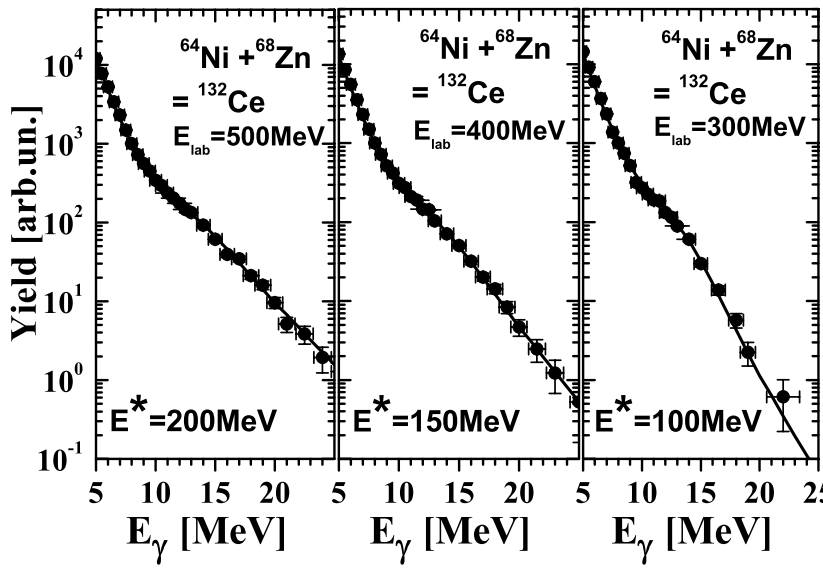

Fig. 3. The measured (filled points) and calculated statistical model (full drawn line) high energy γ-ray spectra for ^{132}Ce at $E^* = 200$, 150 and 100 MeV. The calculations assume a fully thermalized CN and an average spin $\langle J \rangle$ of $45\hbar$. The resonance width and centroid were treated as free parameters of the fit.

these energy spectra. As standard for the analysis of the GDR γ-decay spectra, statistical model calculations were performed to fit the data.

The first important input for the statistical model calculations is the excitation energy of the compound nucleus. In fact, at the basis of the statistical model analysis of the high energy gamma-ray spectra there is the assumption that the GDR vibration at finite temperature is built on the fully thermalized nucleus so that its gamma decay follows statistical laws. For this reason it is important to examine the spectral shape of the alpha spectra measured with the same experimental conditions of the gamma-ray spectra. In the lower panels of Fig. 4 a number of measured spectra of alpha particles corresponding to different angles in the c.m. system are shown for the reaction $^{64}\mathrm{Ni} + {}^{68}\mathrm{Zn}$ at beam energy $E_{\mathrm{lab}} = 500$ MeV. These spectra are compared with the corresponding spectra measured with the reaction $^{16}\mathrm{O} + {}^{116}\mathrm{Sn}$ at beam energy $E_{\mathrm{lab}} = 250$ MeV (upper panels of Fig. 4). Both systems are leading to the same CN, namely ^{132}Ce having by kinematics and under the assumption of full thermalization the same excitation energy of 200 MeV. However, only in the case of the reaction $^{64}\mathrm{Ni} + {}^{68}\mathrm{Zn}$ the alpha spectra are described by statistical model predictions, shown in Fig. 4 with the continuous lines. In addition, the angular distribution of the alpha particle emission is consistent with statistical decay only for the $^{64}\mathrm{Ni} + {}^{68}\mathrm{Zn}$ reaction while that measured for the $^{16}\mathrm{O} + {}^{116}\mathrm{Sn}$ reaction, being strongly peaked at forward angles, has the typical behavior of pre-equilibrium emission. The total energy loss in the excitation energy was found to

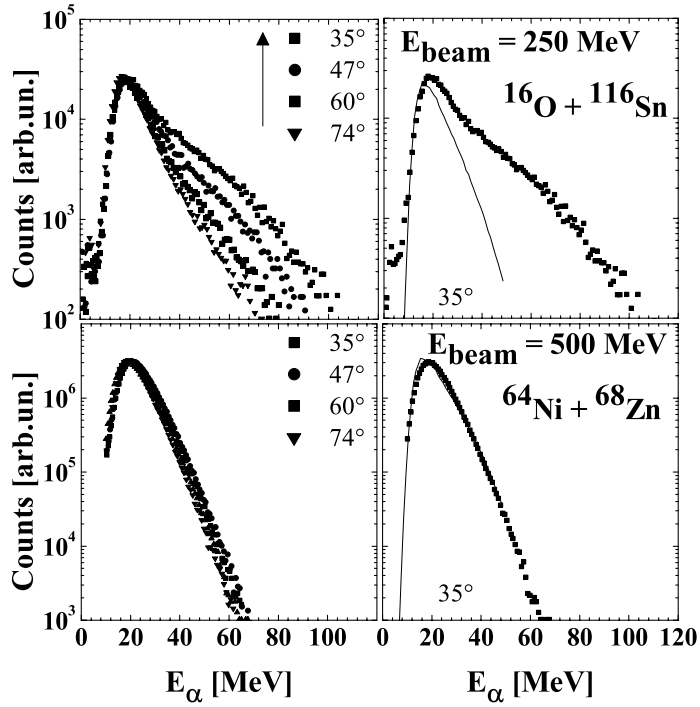

Fig. 4. Left panels: Measured α-spectra in the c.m. system at different angles. The lower panels show the data taken with the ^{64}Ni-beam ($E_{\rm lab}$ = 500 MeV) and the upper panels show data with the ^{16}O-beam ($E_{\rm lab}$ = 250 MeV). The right panels show the spectra specifically at 35°. Both systems are leading to the same CN, namely ^{132}Ce having by kinematics and under the assumption of full thermalization the same excitation energy of 200 MeV. The continuous lines show the statistical model calculations for the decay of ^{132}Ce at E^* = 200 MeV.

be approximately 40 MeV.[16,17] Therefore for the study of the GDR properties at finite temperature we have focused on the analysis of the high-energy gamma-rays from the ^{64}Ni + ^{68}Zn reaction for which the alpha particle spectra show that the center-of-mass energy is entirely given to the equilibrated compound nucleus so that the giant dipole vibration can be assumed to be built on a fully thermalized system.

The high-energy gamma-ray spectrum is produced by the de-excitation of the compound nucleus and of all the other nuclei populated in its decay cascade.[20,21] The GDR strength function was assumed to have the shape of a single Lorentzian function. The resonance width and centroid were treated as free parameters of the fit. In particular, the single Lorentzian strength function was centered at $E_{\rm GDR} \approx 14$ MeV as in Ref. 22 and the GDR excitation was assumed to exhaust 100% of the energy-weighted sum rule (EWSR) strength. For the angular momentum of the compound nucleus we have used for all three different excitation energies a triangular shape distribution with diffuseness corresponding to $2\hbar$. The maximum

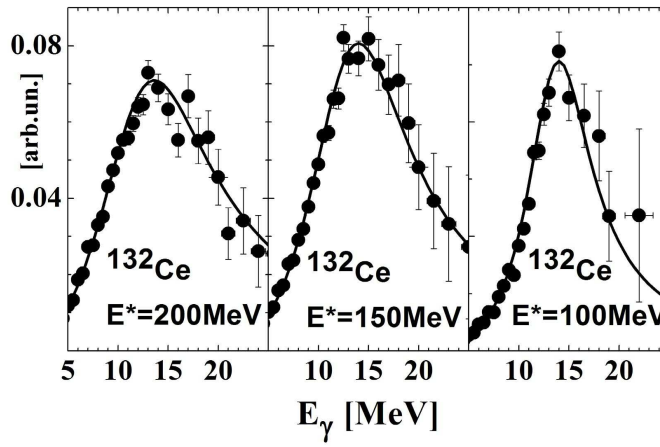

Fig. 5. The quantity $F(E_\gamma)Y_\gamma^{\rm expt}(E_\gamma)/Y_\gamma^{\rm cal}(E_\gamma)$ is plotted for the measurement of ^{132}Ce at $E^* = 200$, 150 and 100 MeV. $Y_\gamma^{\rm expt}(E_\gamma)$ is the experimental spectrum and $Y_\gamma^{\rm cal}(E_\gamma)$ the best fit calculated spectrum of Fig. 3, corresponding to the single Lorentzian function $F(E_\gamma)$. The latter is shown in the figure with the continuum line.

angular momentum of this distribution does not change with the bombarding energies of the present experiment. In fact, the maximum angular momentum that the CN can sustain without fissioning has reached the largest possible value $L_{\rm max} = 70\hbar$ already at bombarding energies lower than the present ones. For the level density description the Reisdorf formalism of Ignatyuk[23–25] was used with a value of the level density parameter a (MeV^{-1}) between $A/10$ and $A/9$ for $E^* < 100$ MeV. At higher excitation energies we used a level density parameter, as deduced from Refs. 26 and 27 which decreases linearly to $A/11$ up to $E^* < 170$ MeV and saturates down to $A/12.5$ for $E^* > 170$ MeV.

The gamma-ray spectra calculated with the statistical model were folded with the response function of the BaF_2 array calculated using the GEANT[28] libraries and were then normalized at around 8 MeV. The width of the Lorentzian function was obtained from the best fit to the data using a χ^2 minimization procedure in the spectral region between 12–22 MeV. Due to the exponential nature of the γ-ray spectra, the χ^2 of this fit is dominated by the low energy part and it is relatively insensitive to the high energy region. Consequently, the best fitting GDR parameters were chosen to be those minimizing the χ^2 divided by the number of counts as, for example, in Ref. 11. The best fitting statistical model calculations (full line) are shown in Fig. 5 in comparison with the experimental results.[15] In order to display the measured and calculated spectra on a linear scale to emphasize the GDR region, the quantity $F(E_\gamma)Y_\gamma^{\rm expt}(E_\gamma)/Y_\gamma^{\rm cal}(E_\gamma)$ was obtained and is displayed in Fig. 5. In particular, $Y_\gamma^{\rm expt}(E_\gamma)$ is the experimental spectrum and $Y_\gamma^{\rm cal}(E_\gamma)$ the best fitting calculated spectrum, corresponding to the single Lorentzian function $F(E_\gamma)$. The best fitting values deduced from the analysis of the GDR region correspond to a width $\Gamma_{\rm GDR} = 8 \pm 1.5$, 12.4 ± 1.2 and 14.1 ± 1.3 MeV at $E^* = 100$, 150, 200 MeV, respectively.

4. The GDR Width and the Model Predictions

In order to compare the values of the GDR width extracted from the experiment with the theoretical prediction, one has to convert the excitation energy of the nucleus emitting the GDR γ-rays into temperature. In particular due to the nature or the measured spectrum one has to average the nuclear temperature over several decay steps. To deduce the nuclear temperature T we have used the expression $T = 1/[d(\ln(\rho))/dE]$, as discussed in Refs. 8, 29 and 30, where ρ is the level density. The resulting values for the present data are not substantially different from those calculated using the expression $T = [(E^* - E_{\rm rot} - E_{\rm GDR})/a)]^{1/2}$, where $E_{\rm rot}$ is the rotational energy.

To each measured γ-ray spectrum it was associated an effective temperature, taking into account in the best possible way the averaging over several decay steps. This averaging becomes more and more important as the excitation energy of the compound nucleus increases. In fact, high energy γ-rays do not come only from the hot compound in the first steps of its deexcitation but are also emitted, with decreasing probability, during all the decay steps of the excited nucleus towards the ground state.

The measured GDR widths (extracted from the high energy γ-ray spectra) consequently will not reflect the properties of the initial nucleus formed with the fusion reaction but rather an average over all the decay paths. Because the shape of the spectra emitted at different temperatures are rather different, it is important to make an appropriate average, which takes into account also the change in the spectral shape. This is equivalent to define an effective temperature corresponding to the average over a temperature region where there is a sensitivity in the fit with the statistical model of the experiment.

In Table 1 the temperature of the CN $T_{\rm CN}$ is given together with the two other temperatures, $\langle T \rangle$ and $T_{\rm eff}$. The values of $\langle T \rangle$ are obtained by averaging the temperatures of all nuclei involved in the decay weighted by their γ-ray yield at high energy, namely between 12–20 MeV, without any temperature threshold. In contrast, to obtain the effective temperature $T_{\rm eff}$ we have used the following procedure.

Table 1. In the first three columns the beam energy, the excitation energies deduced from kinematics and the average spin are listed for the ^{64}Ni-induced reactions. The extracted GDR parameters (in MeV) from the statistical model analysis described in the text are listed in columns 4 and 5. The temperature of the compound nucleus $T_{\rm CN}$ for the ^{64}Ni-induced reactions is listed in column 6. Columns 7 and 8 give the effective T^* and the average temperature $\langle T \rangle$, as discussed in the text.

^{64}Ni $E_{\rm beam}$	E^*	$\langle J \rangle$	$\Gamma_{\rm GDR}$	$E_{\rm GDR}$	$T_{\rm CN}$	$T_{\rm eff}$	$\langle T \rangle$
500 MeV	200 MeV	$45\hbar$	8 ± 1.5	14	4.1	3.7	2.9
400 MeV	150 MeV	$45\hbar$	12.4 ± 1.2	14	3.2	2.8	2.2
300 MeV	100 MeV	$45\hbar$	14.1 ± 1.3	14	2.2	1.9	1.8

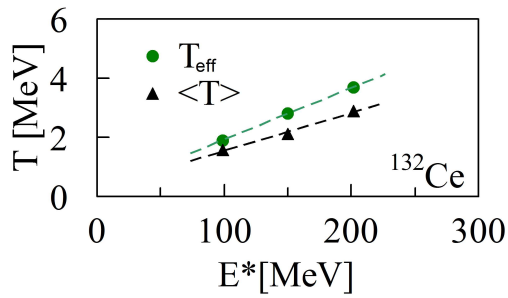

(a)

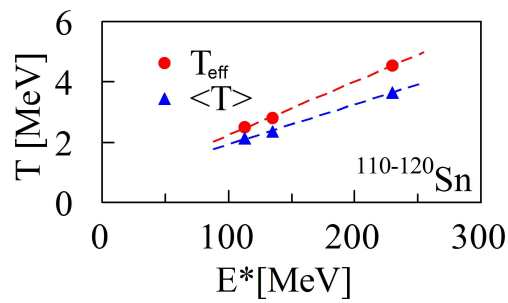

(b)

Fig. 6. The "effective" temperature $T_{\rm eff}$ (filled circles) and the overall average temperature $\langle T\rangle$ (filled triangles) as a function of the excitation energy for the $A = 132$ Ce compound (a) and for the $A = 120$ Sn compound system (b). The "effective" temperature for the GDR is obtained as explained in the text.

Firstly, we have determined the threshold temperature T_s below which a significant change of the GDR width does not affect the width of the total spectra. From the statistical point of view this implies that the χ^2 values remain within the intrinsic statistical uncertainties making the two spectra undistinguishable. Secondly, we have calculated an "effective" temperature $T_{\rm eff}$ which is defined as the temperature at which there is 50% of the high energy γ-ray yield (12–20 MeV) which is emitted between the temperature T_s and the temperature of the initial compound $T_{\rm CN}$. One can notice from Table 1 that up to roughly 2 MeV there is no difference between $\langle T\rangle$ and $T_{\rm eff}$ and that the difference between these two quantities increases with excitation energy.

In order to compare the present results for ^{132}Ce with the existing ones for Sn isotopes we have also determined in this case the effective temperature with the same procedure. The obtained values for the Sn case are shown in Fig. 6(b) in comparison with the effective temperatures of ^{132}Ce (Fig. 6(a)).

The comparison between the measured and predicted evolution of the GDR width as a function of temperature is shown in Fig. 7 for the case of Ce (a) and for Sn (b). The predictions for the Ce nucleus are for $\langle J\rangle = 45\hbar$, value corresponding

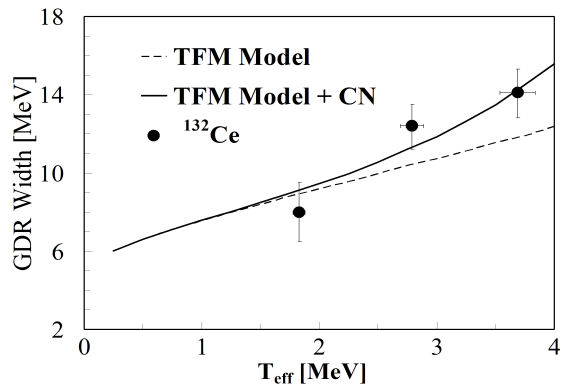

(a)

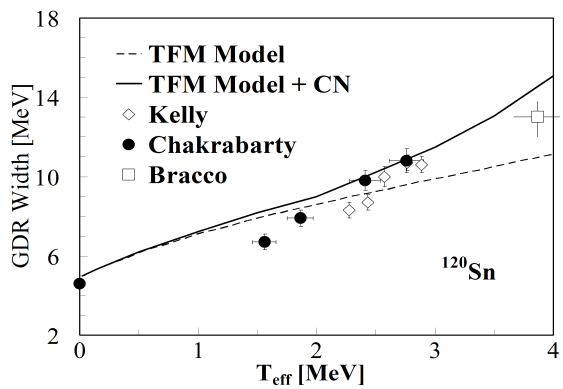

(b)

Fig. 7. Comparison between the measured and predicted evolution of the GDR width as a function of temperature for the case of (a) Ce and (b) Sn. The predictions for the Ce nucleus are for $\langle J \rangle = 45\hbar$ and for Sn are at $\langle J \rangle = 40\hbar$. The measured widths of the GDR are plotted against the effective nuclear temperature of the compound system. The thin continuous lines show the predictions of the thermal shape fluctuation model while the thick continuous lines include also the CN lifetime. For the Sn isotopes the zero temperature value is also shown.

to the reactions used for ^{132}Ce and for Sn are at $\langle J \rangle = 40\hbar$, value corresponding to the data on Sn. The measured widths of the GDR are plotted against the effective nuclear temperature of the compound system. In the case of the ^{132}Ce data the error bars in the width represents the statistical errors connected to the χ^2 minimization. The horizontal bar represents the average temperature range associated to 75% (lower value) and 25% (upper value) of the γ-yield. The neglected yield in the average represents the decay at the end of the CN cascade that is not sensitive to the GDR width because of its spectra shape. In the case of Sn the existing data are plotted at the values of the deduced effective temperatures and the error bars are those reported in the work in Ref. 8. The thin continuous lines show the predictions

of the thermal shape fluctuation model while the thick continuous lines include also the CN lifetime. For the Sn isotopes data at temperatures larger than 2 MeV the pre-equilibrium energy loss due to evaporation of light charged particles in the early stage of the fusion process was estimated as reported in Ref. 8. No pre-equilibrium subtraction was made for the fusion reactions at lower excitation energies from the experiment of Ref. 10. For the Sn isotopes, the zero temperature value is also shown in Fig. 7.

Within the thermal shape fluctuation model the GDR strength function was calculated by averaging the line shape corresponding to the different possible deformations. The averaging over the distribution of shapes is weighted with a Boltzmann factor $P(\beta,\gamma) \propto \exp(-F(\beta,\gamma)/T)$ where F is the free energy and T the nuclear temperature.[2] At each deformation point the width is $\Gamma(\beta,\gamma) = \Gamma_0(E_{\mathrm{GDR}}(\beta,\gamma)/E_0)^{\delta}$, where Γ_0 is the intrinsic width of the giant dipole resonance chosen equal to the zero temperature value, namely 4.5 MeV. With this value of the intrinsic width one generally reproduces rather well the majority of the existing data at $T < 2.5$ MeV.

In both Ce and Sn cases, the predictions account only partially for the GDR width increase measured at $T > 2.5$. Indeed by examining Fig. 7 one can note that at $T > 2.5$ MeV there is a discrepancy between the theory and experimental data. A possible explanation for this discrepancy could be related to the contribution of the lifetime of the compound nucleus which plays a role at these high temperatures. This effect was originally discussed in Refs. 34–36 and was here calculated for these cases. The thick continuous lines include the combined effect of thermal shape fluctuation plus the compound nucleus lifetime. The procedure adopted for summing the different contributions is that described in Ref. 35, namely in the thermal fluctuation averaging at each point for the intrinsic width we use the expression $\Gamma_{\mathrm{GDR}} = \Gamma_0 + 2 * \Gamma_{\mathrm{CN_{evap}}}(T)$ where $\Gamma_{\mathrm{CN_{evap}}}(T)$ is the CN contribution at a given temperature.[34] Such calculations were made not only for Ce but also for Sn. In this way it is possible to compare consistently the GDR width in cerium and tin.

A remarkable agreement between the experimental data and the predictions is found, for both, the $A = 130$ Ce and $A = 120$ Sn cases. From the present comparison one can also note that, in agreement with the expectation of the theory,[2] for $T > 2$ MeV there is no room for a significant increase of the intrinsic width Γ_0 with temperature,[37] unless one unrealistically neglects the CN lifetime contribution to the total width.

The GDR width does not saturate at $T > 2.5$ MeV but increases steadily with temperature at least up to 4 MeV. Deformation effects and the intrinsic lifetime of the compound nucleus are the two combined mechanisms which explain the measured increase of the width with temperature. It is interesting to see how the average nuclear deformation $\langle\beta\rangle$[38] increases with temperature for these two nuclei. For this reason the average deformation was calculated for the same nuclear shape distributions used to deduce the GDR width within the thermal shape fluctuation model. These values are displayed in Fig. 8. One can see that there is a steady increase of the average deformation with temperature which at $T > 2.5$ is not as

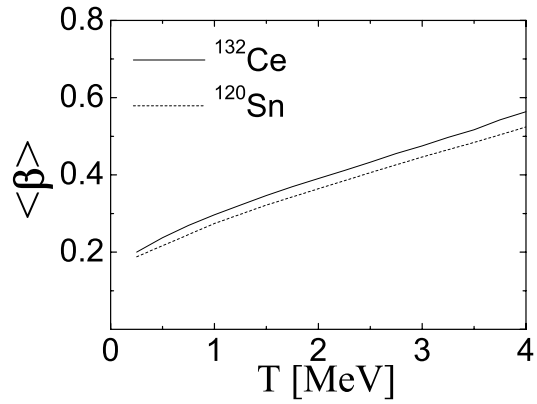

Fig. 8. The line shows the average nuclear deformation $\langle\beta\rangle$ calculated by the TFM for hot $A = 132$ Ce and $A = 120$ Sn. The predicted deformation increase follows the increase of the width of the compound nucleus induced by temperature.

sharp as that of the measured GDR width. In addition by comparing this figure with the calculations of Fig. 6 one can note that the evolution of the GDR width predicted by the thermal fluctuation model mirrors the evolution of the average nuclear deformation.

5. Conclusion

In this paper we have discussed the problem of the GDR width in the temperature interval between 2 and 4 MeV, in connection with the Ce nuclei, for which recent exclusive measurements were made and with Sn isotopes, for which several more inclusive measurements exist. In both cases the experiments at this temperature region correspond to the same angular momentum interval and therefore angular momentum effects are saturated. The analysis of the data shows that the GDR width does not saturate at $T > 2.5$ MeV but increases steadily with temperature at least up to 4 MeV. This behavior is consistent with the one found for the Sn isotopes. In the case of the Ce data the thermalization was well determined by measuring simultaneously in the same experiment light charged particle spectra and γ-rays.

The GDR width in the two mass regions of Sn and Ce is found to consistently increase with temperature. Deformation effects and the sizable contribution of the intrinsic lifetime of the compound nucleus are the two combined mechanisms which explain the measured increase of the GDR width with temperature. This finding sheds more light on the interesting problem of the damping mechanisms of collective modes at finite temperature. However, more exclusive studies such as that of Ce should also be made in other mass regions including more exotic ones, or in other rotational frequency regimes to further test nuclear structure under extreme temperature condition and to learn more about nuclear deformation.

Acknowledgments

The work has been supported by the Italian Institute of Nuclear Physics, U.S. Department of Energy by the University of California, Lawrence Livermore National Laboratory under contract No. W-7405-Eng-48.

References

1. D. Kusnezov and W. E. Ormand, *Phys. Rev. Lett.* **90**, 042501 (2003).
2. P. F. Bortignon, A. Bracco and R. A. Broglia, *Giant Resonances*: *Nuclear Structure at Finite Temperature* (Harwood Academic Publishers, 1998).
3. M. Gallardo *et al.*, *Nucl. Phys. A* **443**, 415 (1985).
4. F. Camera *et al.*, *Nucl Phys. A* **572**, 401 (1994).
5. M. Matiuzzi *et al.*, *Phys. Lett. B* **364**, 13 (1995).
6. P. Donati *et al.*, *Phys. Lett. B* **383**, 15 (1996).
7. J. H. Le Faou *et al.*, *Phys. Rev. Lett.* **72**, 3321 (1994).
8. M. P. Kelly *et al.*, *Phys. Rev. Lett.* **82**, 3404 (1999).
9. M. P. Kelly *et al.*, *Phys. Rev. C* **56**, 3201 (1997).
10. D. R. Chakrabarty *et al.*, *Phys. Rev. C* **36**, 1886 (1987).
11. A. Bracco *et al.*, *Phys. Rev. Lett.* **62**, 2080 (1989).
12. R. J. Voijtech *et al.*, *Phys. Rev. C* **40**, R2441 (1989).
13. G. Enders *et al.*, *Phys. Rev. Lett.* **69**, 249 (1992).
14. H. J. Hoffman *et al.*, *Nucl. Phys. A* **571**, 301 (1994).
15. O. Wieland *et al.*, *Phys. Rev. Lett.* **97**, 012501 (2006).
16. V. L. Kravchuk *et al.*, IWM 2006 conference proceedings.
17. S. Barlini *et al.*, submitted to *Phys. Rev. C.*
18. F. Gramegna *et al.*, *Nucl. Inst. Meth. A* **389**, 474 (1997).
19. M. Kmiecik *et al.*, *Phys. Rev. C* **70**, 064317 (2004).
20. F. Pulhofer, *Nucl. Phys. A* **280**, 267 (1977).
21. I. Dioszegi, *Phys. Rev. C* **64**, 019801 (2001) and references therein.
22. D. Pierroutsakou *et al.*, *Phys. Rev. C* **71**, 054605 (2005).
23. W. Reisdorf, *Z. Phys. A* **300**, 227 (1981).
24. A. V. Ignatyuk *et al.*, *Sov. J. Phys.* **21**, 255 (1975).
25. I. Dioszegi *et al.*, *Phys. Rev. C* **63**, 047601 (2001).
26. J. N. De *et al.*, *Phys Rev. C* **57**, 1398 (1998).
27. M. Gonin *et al.*, *Nucl. Phys. A* **495**, 139c (1989).
28. R. Brun *et al.*, CERN Report No. CERN-DD/EE/84-1.
29. M. Kmiecik *et al.*, *Nucl. Phys. A* **674**, 29 (2000).
30. M. Thoenessen, *Riken Rev.* No. 23 (July 1999).
31. E. F. Garman *et al.*, *Phys. Rev. C* **28**, 2554 (1983).
32. R. K. Voijtech *et al.*, *Phys. Rev. C* **40**, 2441 (1989).
33. W. E. Ormand *et al.*, *Nucl. Phys. A* **617**, 20 (1997).
34. W. E. Ormand *et al.*, *Nucl. Phys. A* **614**, 217 (1997).
35. Ph. Chomaz, *Phys. Lett. B* **347**, 1 (1995).
36. Ph. Chomaz, *Nucl. Phys. A* **569**, 569 (1994).
37. A. Bracco *et al.*, *Phys. Rev. Lett.* **74**, 3748 (1995).
38. M. Matiuzzi *et al.*, *Nucl. Phys. A* **612**, 262 (1997).